GEOLOGY

Glaciers in California's Sierra Nevada are likely disappearing for the first time in the Holocene

Andrew G. Jones[1]*, Shaun A. Marcott[1], Jeremy D. Shakun[2], Nathaniel A. Lifton[3,4], Andrew L. Gorin[5,6], Alan J. Hidy[7], Susan R. H. Zimmerman[6,7], Greg M. Stock[8], Tori M. Kennedy[9], Brent M. Goehring[9,10], Marc A. Caffee[3,4]

Mountain glaciers are sensitive climate indicators. Glaciers in the western United States are projected to disappear by 2100 CE, but whether they were previously absent in the current interglacial (past 11,700 years) remains debated. Here, we present evidence that two of the largest glaciers in California's Sierra Nevada near Yosemite National Park persisted throughout the Holocene. Cosmogenic in situ carbon-14 and beryllium-10 exposure dating in newly exposed proglacial bedrock indicates continuous Holocene cover, likely by ice. At a nearby smaller glacier, bedrock exposure-burial ages suggest glacier expansion at ~7 thousand years ago, earlier than previously recognized. Moraine exposure ages at these sites and the Sierra Nevada's largest glacier are distributed across the past several thousand years, suggesting that glaciers were near their preindustrial extent for much of the late Holocene. These findings imply that a glacier-free Sierra Nevada is unprecedented since before the Holocene. Future alpine glacial environments in California are thereby likely a no-analog scenario within the current interglacial.

INTRODUCTION

Mountain glaciers respond to climate through changes in their length (*1*, *2*). They are iconic features of the United States National Park System such as Yosemite National Park in California, Glacier National Park in Montana, and Grand Teton National Park in Wyoming. Today, glaciers in Yosemite are small fractions of their size when flowing ice was first documented there in the late 19th century (Figs. 1 and 2 and figs. S1 to S3) (*3*). Shrinking glaciers in the western United States are public-facing emblems of climate change, affecting freshwater storage (*4*), river runoff (*5*), and biodiversity (*6*–*8*). Small (<1 km^2) alpine glaciers similar to many across the American West were recently projected to disappear by 2100 CE under most global greenhouse gas emissions pathways (*9*).

It remains unresolved whether a fully deglaciated western United States is anomalous within the multi-millennial context of the Holocene (past 11,700 years or 11.7 kyr). Canonically, glaciers in the western United States are thought to have been absent during the early Holocene and active during "Neoglacial" cooling in the late Holocene (*10*–*13*). In California's Sierra Nevada, low-to-undetectable rock flour levels in lake sediment records downstream of present-day glaciers (*14*, *15*) have been interpreted to indicate glacier absence from 10 to 3 thousand years ago (ka). In Glacier National Park, downstream lake sediment records indicate that Neoglacial advances began at 6.5 ka (*16*). In Grand Teton National Park, however, recent evidence suggests that glaciers persisted through early Holocene summer warmth as rock or debris-covered glaciers before reactivation at 6.3 ka (*17*). Debris-covered glaciers are defined by having a mantle of debris over some fraction of their ablation area that mitigates summer melt via an insulating effect on glacial ice (*18*). Supraglacial debris has been shown to cause nonlinear responses to climate change (*19*) and also has been identified as an important factor in allowing California's glaciers to maintain stable mass balance under adverse climate conditions (*20*). Debris cover is common in the western United States and is difficult to account for in large-scale models (*9*), but well suited for investigation by reconstructing past glacier change.

Here, we contribute to this debate with constraints on the Holocene history of glaciers in California's Sierra Nevada from cosmogenic in situ ^{14}C-^{10}Be concentrations in proglacial bedrock and moraine boulder ^{10}Be exposure ages. The two techniques provide complementary insight: in situ ^{14}C-^{10}Be exposure ages from proglacial bedrock in modern glacier forefields constrain periods of reduced ice extent, whereas moraine boulder exposure ages reflect glaciers' most recent maximum extents. These data are from four of the largest and presumably longest-lived glaciers in the Sierra Nevada—the Conness, Maclure, Lyell, and Palisade glaciers—which span much of its glacierized range (Fig. 1 and fig. S4). The longevity of these glaciers in the face of industrial-era warming makes them bellwethers for investigating Holocene glacier disappearance in the western United States.

Latest Pleistocene and Holocene glacial history

The latest Pleistocene and Holocene glacial history of the Sierra Nevada is defined by two moraine sets: the Recess Peak moraines and the Matthes moraines (*12*). The Recess Peak advance dates to ~13 ka and is the final Pleistocene advance in California (*21*–*23*). Subsequent warming and drying into the Holocene caused recession to positions inboard of the Matthes moraines (*24*), which are generally considered to be the latest Holocene in age—i.e., Little Ice Age (LIA) (*14*). The Recess Peak advance occupied roughly twice the area of the Matthes advance, and there is a coherent relationship between the two generations of moraines across the Sierra Nevada that indicates that these moraines reflect regional-scale climate change (*21*).

[1]Department of Geoscience, University of Wisconsin-Madison, Madison, WI 53706, USA. [2]Department of Earth and Environmental Sciences, Boston College, Chestnut Hill, MA 02467, USA. [3]Department of Earth, Atmospheric, and Planetary Science, Purdue University, West Lafayette, IN 47907, USA. [4]Department of Physics and Astronomy, Purdue University, West Lafayette, IN 47907, USA. [5]Department of Earth and Planetary Science, University of California-Berkeley, Berkeley, CA 94720, USA. [6]Berkeley Geochronology Center, Berkeley, CA 94709, USA. [7]Center for Accelerator Mass Spectrometry, Lawrence Livermore National Laboratory, Livermore, CA 94550, USA. [8]National Park Service, Yosemite National Park, El Portal, CA 95318, USA. [9]Department of Earth and Environmental Sciences, Tulane University, New Orleans, LA 70118 USA. [10]Los Alamos National Laboratory, Los Alamos, NM 87545, USA.
*Corresponding author. Email: agjones3@wisc.edu

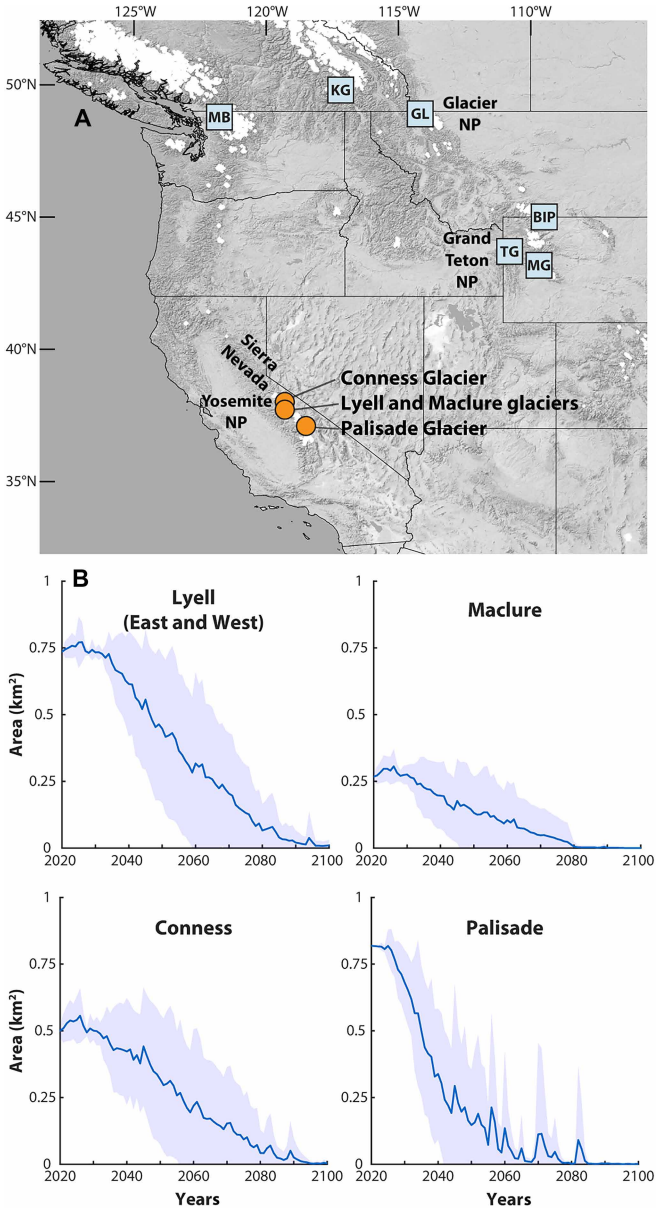

Fig. 1. Site map and glacier area projections to 2100. (**A**) Digital elevation map of western North America with glacierized areas from Randolph Glacier Inventory mapped in white (*66*). Orange circles denote the locations of the glaciers in this study. Blue squares denote the locations of glaciers and ice bodies in studies referenced in the text. TG: Teton Glacier, Wyoming (*17*); BIP: Beartooths Ice Patch, Montana (*58*); GL: Glacier National Park lakes, Montana (*16*); MB: Mt. Baker, Washington (*49*); MG: Mammoth Glacier, Wyoming (*36*); KG: Kokanee Glacier, British Columbia (*36*). The Mammoth and Kokanee glaciers are sites with proglacial bedrock ^{14}C-^{10}Be data shown in Fig. 4. Relevant national parks (NP) are noted on the map. (**B**) Area projections for the glaciers in this study under intermediate (RCP 4.5) warming scenario from 10-model ensemble means (blue line) with SD (shading) (*9*). Base map: Esri World Physical Map (source: US National Park Service).

Within the Holocene, the overall trends in Sierra Nevada glacier change are well defined, but detailed and well-dated records of glacier length are lacking. Alpine glaciers are sensitive to summer temperatures and winter precipitation. Summer insolation over the western United States peaked at ~10 ka and decreased to its Holocene low at 0 ka, while winter precipitation increased in the late Holocene (*25*). Throughout western North America and Europe, moraine exposure dating, dendrochronology (glacial tree-kill dates), and lake sediment records support minimum glacier positions in the early Holocene and maximum positions in the late Holocene (*26*, *27*), with the largest advance likely occurring at the end of the LIA (1300 to 1850 CE) before the onset of industrial-era warming (*21*, *28*). However, precisely how far glaciers retreated in the early and mid-Holocene—and whether they disappeared entirely (*10*)—remains difficult to resolve because the expansive LIA glacier advances likely reworked end moraines that would otherwise have demarcated earlier glacier extents (*29*, *30*). Glaciogenic sediment fluxes trapped in downstream lakes are used to infer Holocene glacier fluctuations, but these are difficult to link precisely to glacier length. Sediment fluxes to a core site can be affected by sediment trapping in upstream lakes, subglacial sediment storage, glacier erosivity, lake level changes, and other factors and have been shown to increase during both glacier advance and recession (*31*–*33*), requiring validation by other methods.

RESULTS

Site and approach

To reconstruct Sierra Nevada glacier sizes during the Holocene, we measured in situ ^{14}C and ^{10}Be concentrations in 17 samples of proglacial bedrock at the Conness, Maclure, and East Lyell glaciers in California (Materials and Methods). Cosmogenic nuclide concentrations in proglacial bedrock reflect the extent of glaciers in the Holocene (*34*–*38*). When glaciers recede and expose proglacial bedrock, in situ ^{14}C and ^{10}Be are produced in the bedrock at known rates, with nuclide production decreasing exponentially with depth to low values beneath ~3 m of rock or ~10 m of ice. Beyond 3-m depth, low-level production by muons dominates (~1% of total surface production for ^{10}Be and 10% for ^{14}C) and extends tens of meters into the subsurface. If glaciers re-form and bury the bedrock, then ^{14}C decreases rapidly relative to ^{10}Be due to ^{14}C's much shorter half-life (5.7 kyr versus 1.4 Myr). Erosion exhumes more weakly dosed bedrock, lowering concentrations of both nuclides. These three parameters—exposure, burial, and erosion—determine the cosmogenic nuclide concentrations in bedrock at the surface and thus directly reflect past glacier length.

The Lyell and Maclure glaciers are in Yosemite National Park, within a few kilometers of each other, while Conness Glacier abuts Yosemite's border ~20 km to the north. Lyell Glacier was a single ice mass in the late 19th century but has since split into two bodies, East Lyell and West Lyell (Fig. 2). East Lyell Glacier stopped flowing (*39*) and is nearly gone today (<0.05 km^2); it lacks the higher headwall shielding present at the Maclure and Conness glaciers (*40*) that insulates ice against solar radiation. East Lyell Glacier's lower threshold for disappearance limits its utility as an indicator of the presence or absence of the most resilient glaciers in the Sierra Nevada, but its Holocene length trends likely mirror those of other glaciers throughout the region. Therefore, at East Lyell Glacier, we collected bedrock samples along a down-valley transect from the headwall to the Matthes moraine to reconstruct the glacier's length over time. Differences in ^{14}C-^{10}Be ratios between samples in this down-valley transect should reflect different burial durations that each sample experienced as a function of glacier length. At the Conness and Maclure glaciers, we collected bedrock samples exposed within the past decade along the modern ice margin to test whether these larger glaciers previously disappeared during the Holocene (Fig. 3). Changes in glacier length

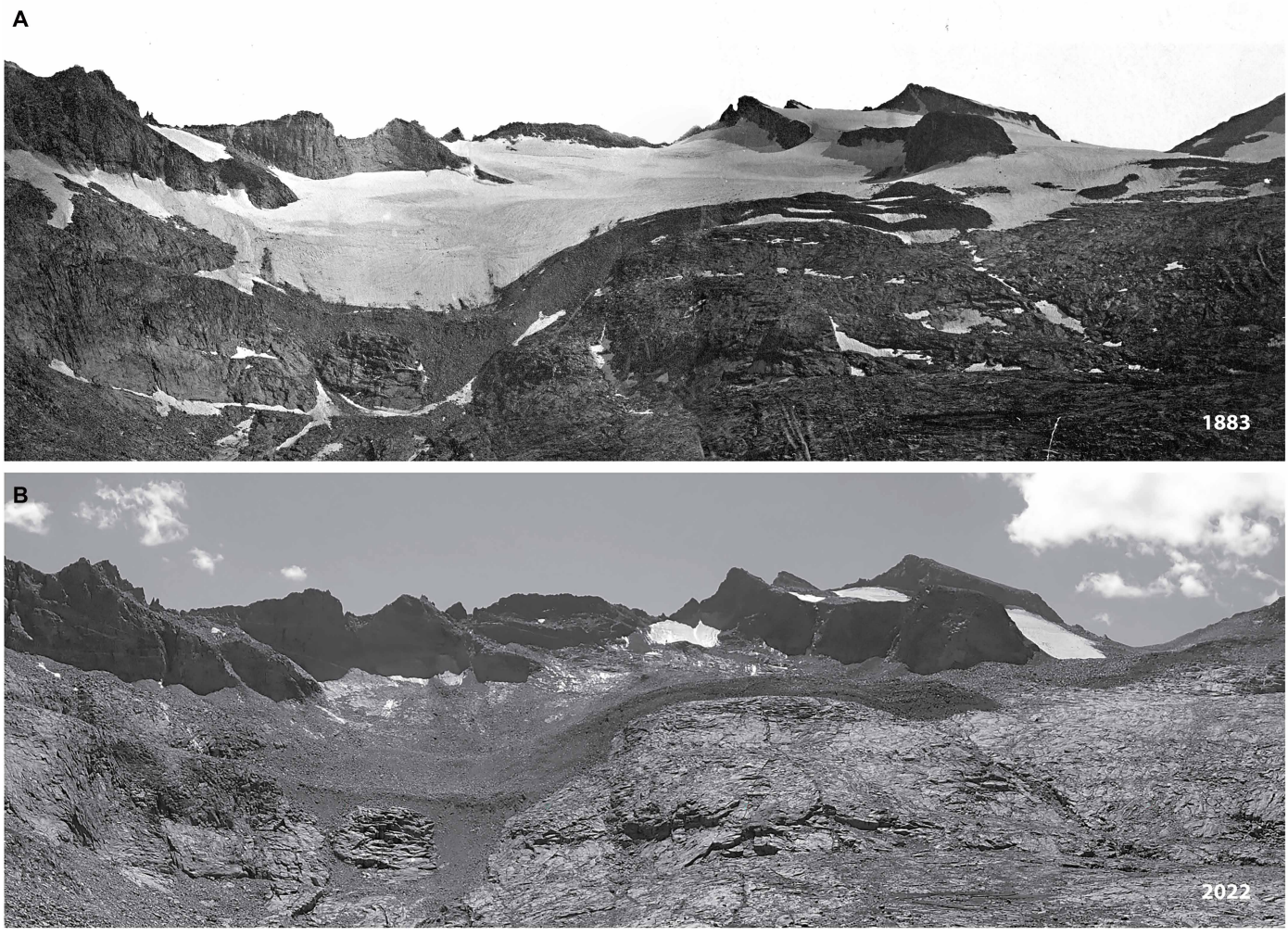

Fig. 2. Repeat photography of East Lyell Glacier. Yosemite National Park, California. (**A**) East Lyell Glacier, Yosemite National Park, in September 1883. Photo credit: I. Russell, United States Geological Survey. (**B**) East Lyell Glacier in September 2022. Photo credit: G. Stock, National Park Service. Note that East (left) and West (right) Lyell lobes were connected in 1883.

likely covered or uncovered all samples along these across-valley transects at once, such that nuclide concentrations should reflect a single ice cover history. We targeted bedrock highpoints for sample collection to minimize the possibility of past burial by debris, water, or prolonged snow cover, rather than glacier ice.

In addition, to better constrain the timing of Holocene glacier maxima, we applied surface-exposure dating with ^{10}Be on 55 moraine boulders on the Matthes moraines of the Conness, Maclure, and Lyell (East and West) glaciers, as well as on Palisade Glacier, the largest glacier in the Sierra Nevada (0.8 km^2) located ~100 km southeast of Yosemite National Park. Glaciogenic sediment records suggest that glaciers were most active during the preindustrial period (*14*, *15*), but the timing of glacial advance to their Matthes positions remains unclear.

Bedrock exposure and moraine ages

Along the Conness and Maclure glacier margins, ^{14}C and ^{10}Be bedrock apparent exposure ages are exceptionally young (all <100 years within 1σ uncertainty; Fig. 3), close to laboratory background values (Supplementary Materials). In the East Lyell Glacier down-valley bedrock transect, exposure ages range from hundreds to thousands of years, with most (six of seven) samples having less than 2 kyr of apparent exposure. In situ ^{14}C ages are lower than ^{10}Be ages at East Lyell, a signature of Holocene exposure followed by burial. The sample closest to the remnant East Lyell Glacier (Lyell-01) reflects 1.7 ± 0.1 kyr (1σ and henceforth) of apparent exposure; this sample's ^{14}C-^{10}Be ratio is compatible with ~8 kyr of burial during the Holocene (Fig. 4). The sample furthest down-valley (Lyell-2023-22) has 7.9 ± 0.4 kyr of apparent exposure; its ^{14}C-^{10}Be ratio is equivalent to ~3 kyr of Holocene burial. Intervening samples have intermediate burial durations. Just outboard of the Matthes moraine, a bedrock sample records 9.3 ± 0.5 kyr of exposure (Fig. 3). This age is considered to reflect the timing of glacier retreat to within LIA limits following deglaciation.

To quantitatively investigate when samples were exposed and buried at the East Lyell forefield—beyond the simple burial durations implied by in situ ^{14}C-^{10}Be ratios alone—we applied a forward model for cosmogenic nuclide evolution in proglacial bedrock (*38*). The

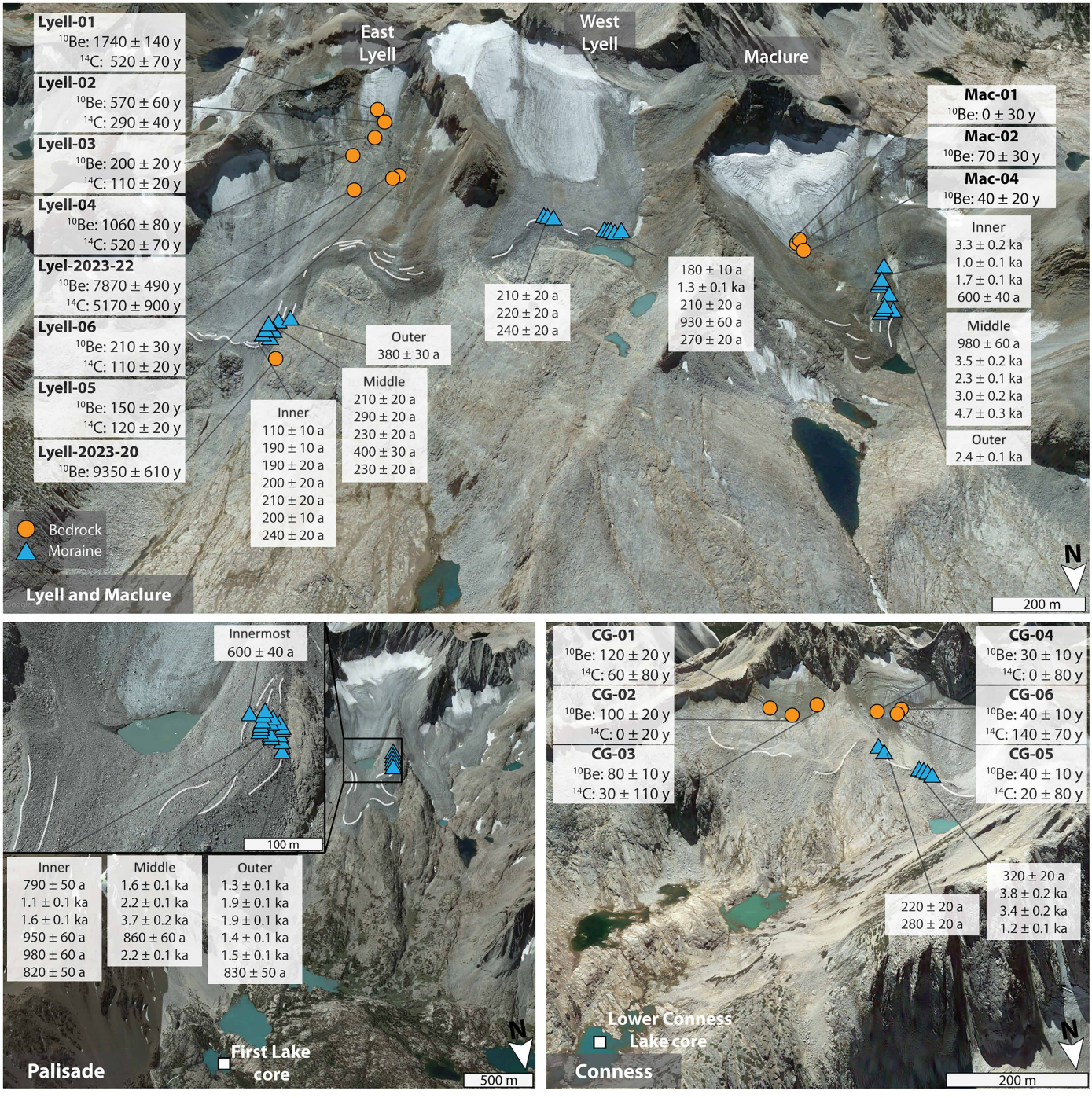

Fig. 3. Oblique satellite imagery showing cosmogenic exposure ages. Glacier forefields with proglacial bedrock in situ ^{14}C-^{10}Be ages and moraine boulder ^{10}Be exposure ages. Bedrock exposure ages are reported as durations of exposure in years ("y"); moraine exposure ages are reported as ages in kiloyears ago ("ka" or "a" when <1 ka). All exposure ages use the LSDn (*64*) scaling scheme. Uncertainties are external (i.e., measurement and production rate uncertainty; 1σ). Matthes moraine ridges mapped with shaded white lines. Lake core locations from prior work (*14*, *15*) indicated with white squares. Satellite imagery from September 2013. Image credit: Google Earth based on Landsat/Copernicus data.

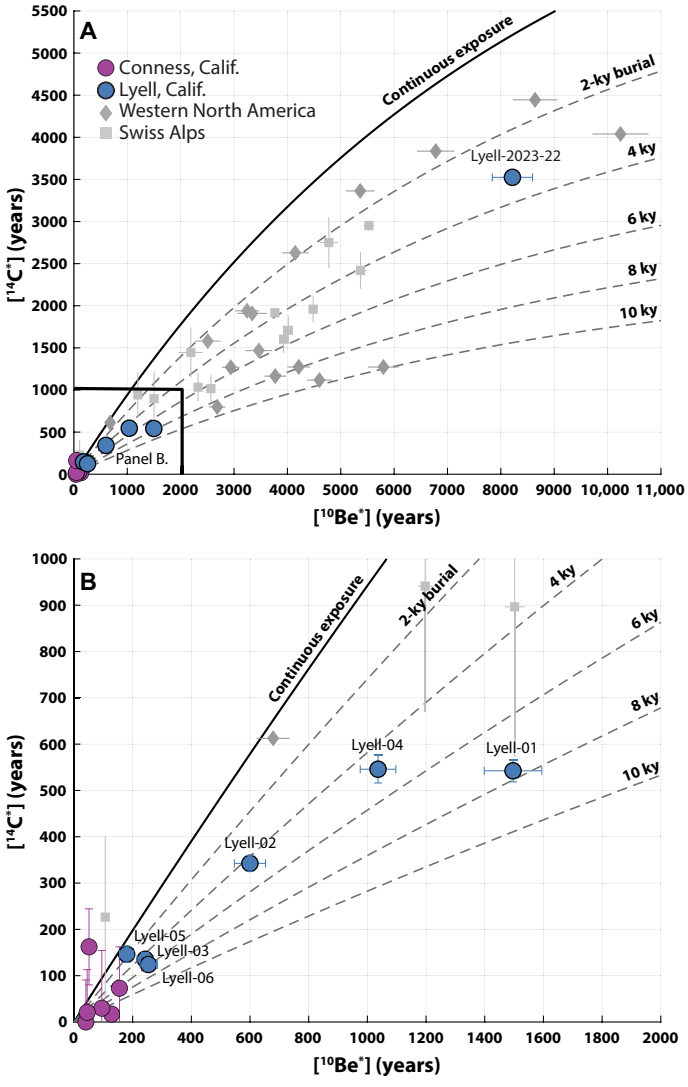

Fig. 4. Two-isotope plot (^{14}C-^{10}Be) with burial isochrons. Bedrock data from the Conness and East Lyell glaciers in this study. Solid line represents continuous exposure; dashed lines represent approximate burial durations after continuous exposure. Nuclide concentrations have been normalized by local production rate to facilitate comparison between sites. Data from western North America are from three glaciers: an unnamed glacier of the Juneau Icefield, Alaska–British Columbia; Kokanee Glacier, British Columbia; and Mammoth Glacier, Wyoming (*36*). Data from the Swiss Alps are from Steingletscher (*37*) and the Rhone Glacier (*34*). Uncertainties are internal (i.e., measurement; 1σ); exposure-burial lines use the LSDn (*64*) scaling scheme. (**B**) is a subplot of (**A**).

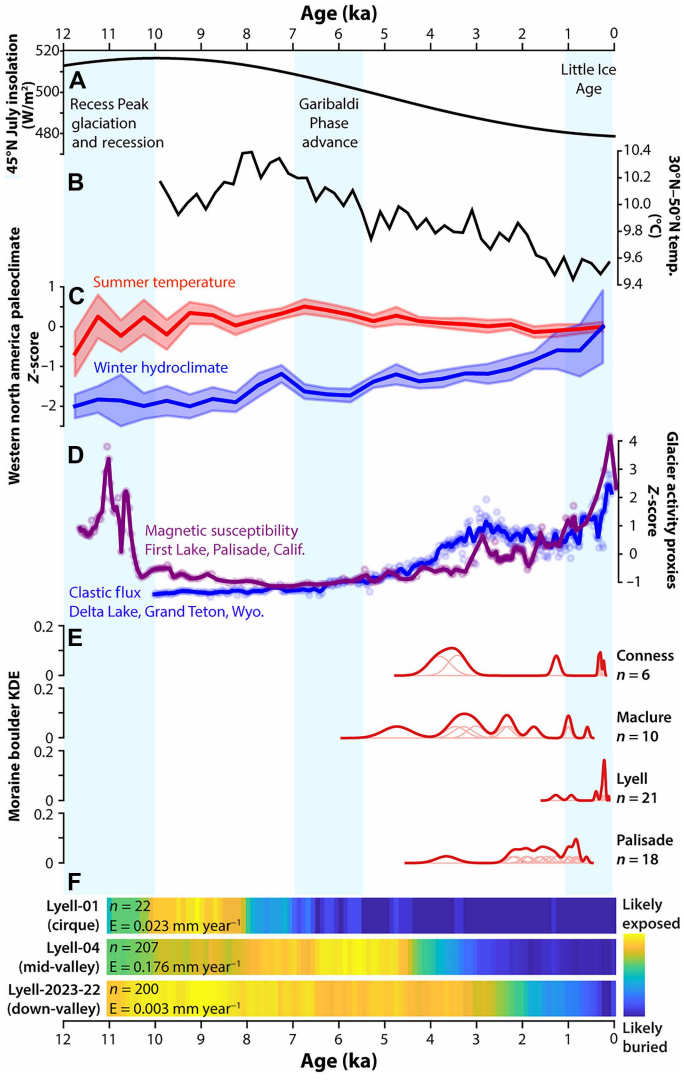

Fig. 5. Holocene paleoclimate and glacier activity. (**A**) 45°N July insolation (*67*). (**B**) Temperature composite from 30°N to 50°N latitudinal band (*51*). temp., temperature. (**C**) Western North America summer temperature and winter hydroclimate data (*25*). (**D**) Magnetic susceptibility from First Lake near Palisade Glacier, California (*14*) and clastic flux record from Delta Lake near Teton Glacier, Wyoming (*17*), with locally weighted scatterplot smoothing (LOWESS). (**E**) Moraine boulder kernel density estimates (KDE; this study). (**F**) Monte Carlo forward model results from three samples at East Lyell Glacier (this study). Yellow is likely exposure; blue is likely burial. The *n* value is number of plausible scenarios at 1σ measurement and production rate uncertainty. "E" refers to the mean erosion rate of these scenarios.

model is used to iteratively identify glacial exposure and burial histories that reproduce each sample's ^{14}C-^{10}Be concentrations under a range of subglacial erosion rates (0.0 to 2.5 mm year^{-1}; Materials and Methods). Model simulations begin at 11 ka. The ^{10}Be sample outboard of the Matthes moraine (9.3 ± 0.5 kyr) limits initial exposure of the samples inboard of the moraine. The highest-elevation sample within the cirque (Lyell-01) is most compatible with exposure from 10 to 8 ka and burial from 7 to 0 ka, while the sample furthest downvalley inboard of the Matthes moraine (Lyell-2023-22) is most compatible with exposure from 11 to 3 ka and burial from 2 to 0 ka (Fig. 5). Among the three highest-exposure samples, there are subsequently later burial dates progressing down-valley from the cirque to the moraine (Fig. 5). The intervening samples exhibit lower nuclide concentrations consistent with higher glacial erosion rates. Lower nuclide concentrations have higher relative uncertainties, which are amplified in nuclide ratio space, and result in a diminished ability to constrain the exposure-burial histories of samples with lower (i.e., <1000 years) apparent exposure (fig. S5).

The Matthes moraines date broadly to the late Holocene rather than exclusively within the LIA (Fig. 3). The (East and West) Lyell Glacier moraine has a mean exposure age of 230 ± 70 a (n = 19), excluding two outliers > 5 SDs from the population mean (*41*). This age is near the end of the LIA, the inferred local glacier maximum. The Conness Glacier moraine has two age populations: the younger

group has a mean age of 270 ± 50 a ($n = 3$), and the older group has a mean age of 2.8 ± 1.4 ka ($n = 3$). The Maclure and Palisade glacier moraines fall within the late Holocene and largely lack LIA exposure ages: only two of 28 boulders dated across the two moraines are within the LIA period. At the Maclure Glacier, the inner moraine ridge age is 1.7 ± 1.2 ka ($n = 4$), and the outer ridge is 3.4 ± 1.0 ka ($n = 4$); at the Palisade Glacier, the inner moraine ridge is 1.0 ± 0.3 ka ($n = 6$), the middle ridge is 2.1 ± 1.0 ka ($n = 5$), and the outer ridge is 1.5 ± 0.4 ka ($n = 6$). The inner moraine ridges at both sites are younger, on average, than the outer ridges.

DISCUSSION

The cosmogenic data are difficult to reconcile with a deglaciated Sierra Nevada

The near-zero ^{10}Be and ^{14}C concentrations we find in recently exposed bedrock along the margins of the Conness and Maclure glaciers could be explained by two scenarios: (i) sample sites were buried throughout the Holocene, preventing the buildup of nuclides, or (ii) the bedrock was deeply eroded following exposure, removing nuclides produced earlier in the Holocene. The scattered late Holocene ^{10}Be ages we obtained on the Matthes moraine boulders could likewise be interpreted in multiple ways—the moraines may have been constructed over the past several millennia, or the glaciers briefly advanced to the moraine positions during the LIA and most of the boulders contain inherited nuclides. Given these various possible interpretations, we first try to explain the cosmogenic data in the context of the prevailing paradigm based on downstream lake sediment records (*14*, *15*) that glaciers in the Sierra Nevada disappeared in the early Holocene and did not reform until ~3 ka.

One interpretation is that there was a thick mantle of rock debris and/or snow across the glacier forefields throughout the Holocene. The rock debris would have absorbed cosmic radiation, producing elevated nuclide concentrations in the debris but none in the underlying bedrock. The LIA glacier advance would have then recycled this nuclide-rich debris during moraine construction, depositing many boulders with inherited nuclides. However, this debris cover scenario is problematic. There are two main sources for debris in these glacier forefields: glacial sediments deposited during glacier recession and nonglacial sediments from rockfall and debris flows (landslides). Regarding glacial deposits, bedrock outboard of the late Holocene moraines is generally debris free (Figs. 2 and 3 and figs. S1 to S3), suggesting that ice retreat after the last deglaciation did not deposit a long-lasting debris mantle over the bedrock. This view is supported by 9.3 ± 0.5 kyr of exposure recorded in the bedrock sample outboard of the Matthes moraine at East Lyell. Rather, the primary source of debris in these glacier forefields is talus emanating from cirque headwalls. Sierra Nevada glaciers receive rockfall from their headwalls (*20*), but in the absence of a glacier to move material downslope, talus accumulation is generally limited to the base of the headwalls (*18*). Our bedrock samples are located tens to hundreds of meters from cirque headwalls, where debris is less likely to accumulate (Fig. 3). Given sufficient time, landslides and rockfall accumulation could grow a talus cone further downslope (*42*), but the near-zero exposure ages in our samples require immediate burial following deglaciation. Furthermore, although scattered debris is common in the forefields today, it is not thick enough (≥3 m) to shield all bedrock from cosmic radiation. Considerable bedrock is exposed, similar to the sites we sampled. Snow can also reduce surface nuclide production (*43*). However, for snowpack alone to explain the measured nuclide concentrations, it would need to persist year-round at depths exceeding 10 m for 10 millennia. These conditions at these locations and slopes would lead to ice, which is now absent from the bedrock sites.

Alternatively, it is possible that nuclides were produced in the bedrock due to exposure before 3 ka, but these nuclides were subsequently removed by subglacial erosion during Neoglacial ice advances. However, this explanation is also difficult to substantiate. Subglacial erosion rates would need to be >0.5 mm year^{-1} to remove an early- to mid-Holocene exposure signal (*36*), which is an order of magnitude higher than estimated abrasion rates at Conness Glacier (0.01 mm year^{-1}) from a power-based abrasion law (*35*). Subglacial quarrying can erode bedrock rapidly compared to abrasion (*44*), but it is a spatially heterogeneous process (*45*, *46*) and is unlikely to have affected all nine samples across both the Conness and Maclure forefields. Glacial erosion rates are also linked to local climate (*47*), ice thickness, slope, and lithology (*48*), which are similar between the nearby Maclure and East Lyell Glacier forefields (~2 km apart).

We highlight five other glacier forefields in western North America (*36*) and the Swiss Alps (*34*, *37*) where in situ ^{14}C-^{10}Be ratios record thousands of years of exposure as evidence that these mechanisms of bedrock burial are secondary influences compared to glacial ice (Fig. 4). Glacial erosion, snow, and scattered debris are ubiquitous features of proglacial environments, but nuclide production still occurs, most notably in our nearby samples at East Lyell Glacier (Fig. 4). The thousands of years of exposure recorded in the East Lyell forefield bedrock thereby provide further support that these variables are not a sufficient explanation for the near-zero exposure ages in the Maclure and Conness glacier forefields.

The glacier length history inferred by the East Lyell bedrock data also casts doubt on the view that glaciers were absent before 3 ka. Forward modeling suggests that the highest-elevation sample within the cirque (Lyell-01) is most compatible with exposure from 10 to 8 ka and burial from 7 to 0 ka, while the sample furthest down-valley inboard of the Matthes moraine (Lyell-2023-22) is most compatible with exposure from 11 to 3 ka and burial from 2 to 0 ka (Fig. 5). The intervening samples suggest a general trend of subsequently later burial dates progressing down-valley from the cirque to the moraine (fig. S5). These exposure-burial histories therefore suggest that East Lyell was only smaller than today during a portion of the early Holocene. The data are concordant with glacial ice forming in the cirque, burying the highest-elevation sample first and then progressively burying more samples as ice advanced down-valley during the Holocene. Progressive glacier expansion beginning between 7 and 6 ka has been documented in numerous locations in western North America (*16*, *17*, *26*, *49*), in some areas referred to as the Garibaldi Phase advance (6.9 to 5.6 ka; Fig. 5) (*50*). Northern midlatitude temperature peaked at ~8 ka and cooled to the LIA, with a similar cooling trend after ~7 ka observed locally in western North American summer temperatures (Fig. 5) (*25*, *51*). Winter precipitation also increased from ~6 ka to the LIA (*25*). These factors together plausibly drove progressive glacier expansion over the mid- to late Holocene. Seasonal snow shielding during winter months could increase the calculated exposure ages by ~10 to 20% (*45*), which would shift the inferred timing of glacier expansion up to ~1 kyr later, but would not alter the interpretation that East Lyell Glacier existed for most of the Holocene.

A revised view on Holocene glaciation in the Sierra Nevada

Given these difficulties in reconciling the cosmogenic data with a deglaciated Sierra Nevada for most of the Holocene, we offer a revised interpretation—the largest glaciers of the Sierra Nevada persisted for the duration of the Holocene, perhaps as rock or debris-covered glaciers at times. Persistent ice cover throughout the Holocene would have prevented nuclide accumulation, explaining the ubiquitously low nuclide concentrations in recently exposed bedrock at Conness and Maclure glaciers. The regional climate history may also support this interpretation of unprecedented glacier retreat today. Summer temperatures in California have warmed ~2°C over the past century, which is comparable to or greater than temperature anomalies that helped drive glacier retreat in the early Holocene (Fig. 5) (*52*, *53*).

Under this framework, Sierra Nevada glaciers expanded at ~7 ka based on the East Lyell bedrock data and were near their Matthes extents for much of the late Holocene based on a simple interpretation of the moraine exposure ages. The spread in exposure ages may relate to the influence of debris on Sierra Nevada glaciers. Debris-covered glaciers have been shown to exhibit anomalously old exposure ages on multiple moraine crests (*19*, *54*). Numerical modeling suggests that these older ages occur because debris mitigates ablation during warming, which can lead to deflation of the terminal moraine rather than ice margin pullback (*55*). The moraine thickens during subsequent cooling rather than being overrun by ice margin readvance, causing greater moraine preservation than in a clean-ice glacier (*15*, *19*). The geomorphology is also consistent with a potentially important role for debris—the hummocky morphology of the Matthes moraines may indicate remnant ice cores (*20*), and the angular boulders that comprise the moraines are suggestive of supraglacial debris fed by rockfall from the surrounding cirque cliffs.

Debris cover on the glaciers may also help reconcile the apparent disagreement between the downstream-lake records that were interpreted to show glacier absence before 3 ka and the persistent Holocene ice cover inferred here from cosmogenic nuclides. Rock and debris-covered glaciers are moving slower than clean-ice glaciers, and low sliding speeds with minimal abrasion (*56*) may explain the lack of visible rock flour (gray glacial sedimentation) in the downstream-lake records from Palisade and Conness glaciers before ~3 ka (*14*, *15*). This interpretation is supported by a similar glacier activity record from the Tetons (*17*). Near Teton Glacier, increasing sediment flux to a downstream lake after 6.3 ka is interpreted as a change from a rock glacier to a more active, abrasive glacier (predicated upon a comparison to a nearby unglaciated catchment). The glacial activity record from Palisade Glacier, based on magnetic susceptibility, resembles the Teton Glacier activity record (Fig. 5). Glacier activity begins to increase between 7 and 6 ka, has a peak near 3 ka, and has a resurgence during the LIA. It is also possible that sediment trapping in upstream lakes diminished an already-weak rock flour signal when glaciers were in reduced positions before the late Holocene. The rock flour records from Conness and Palisade glaciers are from the second and third downstream lakes, respectively, in paternoster lakes (i.e., chains of lakes).

Projected Sierra Nevada glacier disappearance and its implications

Instead of a glacier-free Sierra Nevada in the early and mid-Holocene, our findings suggest that the Sierra Nevada's largest glaciers persisted through most to all of the Holocene. Our interpretation of long-term bedrock burial at the Conness and Maclure glaciers and early mid-Holocene expansion of the East Lyell Glacier contrasts with the previous understanding that Sierra Nevada glaciers were ephemeral features, absent from 10 ka until reappearance at 3 ka (*14*, *15*). The initiation of glacier expansion between 7 and 6 ka brings the Sierra Nevada into alignment with the broader glacial history of western North America. After the initial idea of neoglaciation beginning at 4 ka posited by Porter and Denton (*13*), more recent chronologic constraints have found that western United States glacier expansion likely began around ~6.5 ka (*11*). Glacier advances documented between 7 and 6 ka at Mt. Baker in Washington (*49*), in Grand Teton National Park (*17*), and in Glacier National Park (*16*) support an earlier "neoglaciation," before 4 ka. Within two centuries (~1900 to 2100 CE), the equilibrium line altitude of California's glaciers will have risen from its lowest level of the past 11,700 years to its highest. This recession represents an abrupt reversal of long-term glacier growth over the past ~6500 years. Considering that California's glaciers reached their Last Glacial Maximum positions as early as 30,000 years ago (*23*), our reconstructed glacial history indicates that a future glacier-free Sierra Nevada is unprecedented in human history since known peopling of the Americas ~20,000 years ago (*57*).

Persistent ice during the early Holocene has been documented in Wyoming as a rock glacier (*17*), in Montana's Beartooth Range as an ice patch (*58*), and now in California at the Conness and Maclure glaciers, potentially aided by debris cover. In these locations, warm and dry conditions in the early Holocene made small-glacier survival difficult. This century, as temperatures exceed their Holocene bounds, similar ice bodies in the western United States are projected to disappear. Anthropogenic climate change is therefore likely creating a no-analog scenario in the western United States within the current interglacial.

MATERIALS AND METHODS

Experimental design

We collected bedrock from the forefields of three glaciers in the central Sierra Nevada, California. Cosmogenic nuclide concentrations measured in bedrock between the terminus of modern ice and the preindustrial moraine record changes in glacier size during the Holocene. Conness, Maclure, and East Lyell glaciers are three of the (historically) largest Sierra Nevada glaciers. The forefields abutting the modern glaciers exhibited bedrock exposure that made them ideal sample sites to evaluate past glacier length fluctuations. We targeted local bedrock highpoints to minimize the probability of debris coverage in the past that would influence the measured concentrations (field photos in fig. S6 to S8).

We designed the experiment to test between two end-member scenarios: (i) the scenario presented by the literature (*14*, *23*) that glaciers were absent from 10 to 3 ka, and (ii) the scenario proposed by Larsen *et al.* (*17*) that glaciers persisted (likely as rock or debris-covered glaciers) through the Holocene. In the first scenario, we expect bedrock nuclide concentrations to demonstrate ~7 kyr of exposure, followed by ~3 kyr of burial. In the second scenario, we expect nuclide concentrations to be very low, approaching accelerator mass spectrometry (AMS) system blank concentrations, indicating burial for the duration of the Holocene, and likely longer. The moraine exposure ages constrain the timing of when the glacier occupied its Holocene maximum position. We analyzed the results within the context of the lake sediment records that comprise the primary data for Holocene glacier activity in the Sierra Nevada (*14*, *15*) on updated age models (Supplementary Materials).

Cosmogenic nuclide dating

Quartz separation and ^{10}Be extraction for bedrock samples occurred at the University of Wisconsin-Madison following standard laboratory procedures (*59*, *60*); quartz separation and ^{10}Be extraction for moraine boulder samples occurred at the Lawrence Livermore National Laboratory (LLNL) following standard procedures (*61*). The general procedures from both groups are as follows: rock samples of 1 to 2 kg are crushed and sieved to a 710- to 250-μm size fraction (500 to 250 μm at LLNL). Magnetic minerals are removed via Frantz magnetic separation. Froth flotation is used to remove feldspathic minerals. HCl and weak HF/HNO_3 are used to dissolve remaining nonquartz minerals, remove meteoric ^{10}Be, and etch the quartz. Quartz is partitioned off for ^{10}Be and ^{14}C from the same aliquot. To extract ^{10}Be for AMS measurement, samples were spiked with ^{9}Be carrier of known concentration and dissolved in concentrated HF. Anion/cation exchange chromatography is performed to remove ions that interfere with AMS measurement. Beryllium hydroxide gels are precipitated, dried, and calcined. Beryllium oxide is mixed with niobium powder and packed into cathodes for AMS measurement at Purdue Rare Isotope Measurement (PRIME) Lab for the bedrock samples and LLNL for the moraine boulders. A background correction was made using the mean and SD of process blanks specific to each sample batch (Supplementary Materials).

Gas extraction of ^{14}C took place at Purdue University following the procedures of Lifton *et al.* (*62*). Quartz is etched in 50/50 HNO_3 solution and vacuum dried to minimize atmospheric carbon adsorption. A titanium boat is loaded with 20 g of $LiBO_2$ and degassed at 500°C. Quartz is added to the $LiBO_2$ and dissolved at 1050°C. Carbon dioxide released during dissolution is trapped and passed through a gas exchange line to eventually precipitate carbon as graphite. An aliquot of the gas is stored to measure the ^{14}C:^{13}C ratio, and the ^{14}C:^{13}C ratio is measured on the graphite with the PRIME Lab AMS. A background correction was made using the mean and SD of the process blanks that preceded and followed a sample or set of samples. This value is reported as the effective blank. All laboratory measurement details needed to recalculate nuclide concentrations and exposure ages are available in the Supplementary Materials.

Proglacial bedrock forward model

The evolution of in situ ^{14}C-^{10}Be ratios in bedrock occurs according to a few physical principles that are simulated with a forward model (*38*). This model is governed by Eq. 1

$$N(z, t_i) = P(z) \cdot (\Delta t) + N(z, t_{i-1}) \cdot e^{-\lambda \cdot \Delta t} \quad (1)$$

where N is the nuclide concentration in a theoretical bedrock column as a function of depth (z) and elapsed time (t), i is the current timestep index, P is the total production rate in atoms per gram per year of the nuclide via spallation and muon production as a function of depth, Δt is the timestep duration (100 years), and λ is the nuclide's decay constant. At each timestep, the model simulates one of two conditions: exposure or burial. When bedrock is exposed, nuclides accumulate according to known production rates. Production rates are calculated for each sample as a function of latitude, longitude, elevation, thickness, and topographic shielding, using source code from the CRONUS online calculator (*63*) and the LSDn scaling scheme (*64*). When bedrock is buried under tens of meters of glacial ice, production ceases, erosion of the bedrock surface occurs, and radioactive decay dominates. The forward model iterates through millions of Holocene exposure, burial, and subglacial erosion scenarios to identify those that can reproduce the measured nuclide concentrations. First, a population of 100,000 unique exposure-burial scenarios is generated pseudorandomly. The scenarios are discretized into 110 timesteps of 100 years, totaling 11,000 years (representing 11 to 0 ka). Exposure is represented by "1" and burial by "0," such that each scenario is a vector of 1s and 0s with 110 elements. A range of "glacier oscillation" probabilities (P = 0.6 to 0.99)—that each timestep's condition matches the previous—is used to generate the scenario bank. For example, scenarios generated with P = 0.6 frequently change between 1 and 0, whereas those made with P = 0.99 are highly stable. This range explores the possibility of rapid glacier oscillations over the bedrock and more stable, millennial-scale oscillations. Second, each scenario is simulated at a range of erosion rates from 0.0 to 2.5 mm year^{-1} in steps (0.1 mm year^{-1}), such that the total number of scenarios tested for each sample is 2.6 million (100,000 scenarios × 26 erosion rates). The bedrock columns are discretized into 5000 mm (5 m in total) increments, and erosion is simulated by removing the uppermost bedrock in millimeters at the applied subglacial erosion rate. After all the scenarios are tested, those that replicate measured concentrations within 1σ measurement uncertainty (including production rate uncertainty of 7.3% for ^{14}C and 8.3% for ^{10}Be; 1σ) (*65*) are considered plausible. From this plausible set, the "probability of exposure" at each timestep is calculated by the fraction of scenarios indicating exposure. This process creates a probability of exposure over time for each sample (fig. S5), which reflects when exposure or burial is most likely. Further model details can be found in supplements to Jones *et al.* (*36*) and Vickers *et al.* (*38*).

The Monte Carlo forward model incorporates several geologic assumptions. By running model simulations for 11,000 years, we implicitly assume that there is no pre-Holocene inheritance—that is, no nuclides from past exposure preserved by insufficient glacial erosion during the Last Glacial Maximum. This assumption is consistent with the absence of cosmogenic exposure ages greater than the length of the Holocene from inboard of preindustrial moraines in this study and elsewhere in the western United States (*36*). We assume no erosion during exposure; this is supported by the presence of glacially abraded bedrock in Yosemite National Park exposed after the last deglaciation (~19 to 12 ka), which implies near-zero surface erosion since glacier retreat. We do not consider bedrock exfoliation. All samples are glacially abraded except for two: Lyell-05 and Lyell-06. These samples were in a small zone of exfoliating bedrock of the nondominant lithology within the forefield at East Lyell. Both samples exhibit young exposure ages relative to the nearby Lyell-2023-22, suggestive of deeper erosion perhaps related to the exfoliation. The preserved glacial polish on the other samples suggests that this effect is minimal. Last, we do not consider through-ice nuclide production during burial. We argue that nuclides accumulated under thin ice are negligible based on prior work by Gorin *et al.* (see their fig. S7) (*35*), which demonstrated that nuclide accumulation for 10,000 years through 10 m of ice (normalized to local production rate) would add ~200 years apparent exposure of both ^{14}C and ^{10}Be. Thicker ice would produce even fewer nuclides: production through 30 m of ice would add ~25 years apparent exposure of both ^{14}C (after 10,000 years) and ^{10}Be (after 50,000 years).

Supplementary Materials

The PDF file includes:

Supplementary Text
Figs. S1 to S12
Tables S1 to S4
Legend for data S1
References

Other Supplementary Material for this manuscript includes the following:

Data S1

REFERENCES AND NOTES

1. J. Oerlemans, Extracting a climate signal from 169 glacier records. *Science* **308**, 675–677 (2005).
2. G. H. Roe, M. B. Baker, F. Herla, Centennial glacier retreat as categorical evidence of regional climate change. *Nat. Geosci.* **10**, 95–99 (2017).
3. J. Muir, On actual glaciers in California. *Am. J. Sci. Arts.* **5**, 69–73 (1874).
4. P. Jansson, R. Hock, T. Schneider, The concept of glacier storage: A review. *J. Hydrol.* **282**, 116–129 (2003).
5. V. Radić, R. Hock, Glaciers in the Earth's hydrological cycle: Assessments of glacier mass and runoff changes on global and regional Scales. *Surv. Geophys.* **35**, 813–837 (2014).
6. A. M. Milner, K. Khamis, T. J. Battin, J. E. Brittain, N. E. Barrand, L. Füreder, S. Cauvy-Fraunié, G. M. Gíslason, D. Jacobsen, D. M. Hannah, A. J. Hodson, E. Hood, V. Lencioni, J. S. Ólafsson, C. T. Robinson, M. Tranter, L. E. Brown, Glacier shrinkage driving global changes in downstream systems. *Proc. Natl. Acad. Sci. U.S.A.* **114**, 9770–9778 (2017).
7. S. Brighenti, S. Hotaling, D. S. Finn, A. G. Fountain, M. Hayashi, D. Herbst, J. E. Saros, L. M. Tronstad, C. I. Millar, Rock glaciers and related cold rocky landforms: Overlooked climate refugia for mountain biodiversity. *Glob. Chang. Biol.* **27**, 1504–1517 (2021).
8. S. Cauvy-Fraunié, O. Dangles, A global synthesis of biodiversity responses to glacier retreat. *Nat. Ecol. Evol.* **3**, 1675–1685 (2019).
9. D. R. Rounce, R. Hock, F. Maussion, R. Hugonnet, W. Kochtitzky, M. Huss, E. Berthier, D. Brinkerhoff, L. Compagno, L. Copland, D. Farinotti, B. Menounos, R. W. McNabb, Global glacier change in the 21st century: Every increase in temperature matters. *Science* **379**, 78–83 (2023).
10. P. T. Davis, Holocene glacier fluctuations in the American Cordillera. *Quat. Sci. Rev.* **7**, 129–157 (1988).
11. P. T. Davis, B. Menounos, G. Osborn, Holocene and latest Pleistocene alpine glacier fluctuations: A global perspective. *Quat. Sci. Rev.* **28**, 2021–2033 (2009).
12. F. E. Matthes, Rebirth of the glaciers of the Sierra Nevada during late post-Pleistocene time. *Geol. Soc. Am. Bull.* **52**, 2030–2030 (1941).
13. S. C. Porter, G. H. Denton, Chronology of neoglaciation in the North American Cordillera. *Am. J. Sci.* **265**, 177–210 (1967).
14. N. D. Bowerman, D. H. Clark, Holocene glaciation of the central Sierra Nevada, California. *Quat. Sci. Rev.* **30**, 1067–1085 (2011).
15. S. K. Konrad, D. H. Clark, Evidence for an early Neoglacial glacier advance from rock glaciers and lake sediments in the Sierra Nevada, California, U.S.A. *Arct. Antarct. Alp. Res.* **30**, 272–284 (1998).
16. J. S. Munroe, T. A. Crocker, A. M. Giesche, L. E. Rahlson, L. T. Duran, M. F. Bigl, B. J. C. Laabs, A lacustrine-based Neoglacial record for Glacier National Park, Montana, USA. *Quat. Sci. Rev.* **53**, 39–54 (2012).
17. D. J. Larsen, S. E. Crump, A. Blumm, Alpine glacier resilience and Neoglacial fluctuations linked to Holocene snowfall trends in the western United States. *Sci. Adv.* **6**, eabc7661 (2020).
18. R. S. Anderson, L. S. Anderson, W. H. Armstrong, M. W. Rossi, S. E. Crump, Glaciation of alpine valleys: The glacier – debris-covered glacier – rock glacier continuum. *Geomorphology* **311**, 127–142 (2018).
19. S. E. Crump, L. S. Anderson, G. H. Miller, R. S. Anderson, Interpreting exposure ages from ice-cored moraines: A Neoglacial case study on Baffin Island, Arctic Canada. *J. Quat. Sci.* **32**, 1049–1062 (2017).
20. D. H. Clark, M. M. Clark, A. R. Gillespie, Debris-covered glaciers in the Sierra Nevada, California, and their implications for snowline reconstructions. *Quatern. Res.* **41**, 139–153 (1994).
21. D. H. Clark, A. R. Gillespie, Timing and significance of late-glacial and Holocene cirque glaciation in the Sierra Nevada, California. *Quat. Int.* **38–39**, 21–38 (1997).
22. S. A. Marcott, P. U. Clark, J. D. Shakun, E. J. Brook, P. T. Davis, M. W. Caffee, ^{10}Be age constraints on latest Pleistocene and Holocene cirque glaciation across the western United States. *npj Clim. Atmos. Sci.* **2**, 5 (2019).
23. F. M. Phillips, Cosmogenic nuclide data sets from the Sierra Nevada, California, for assessment of nuclide production models: I. Late Pleistocene glacial chronology. *Quat. Geochronol.* **35**, 119–129 (2016).
24. J. H. Street, R. S. Anderson, A. Paytan, An organic geochemical record of Sierra Nevada climate since the LGM from Swamp Lake, Yosemite. *Quat. Sci. Rev.* **40**, 89–106 (2012).
25. C. C. Routson, D. S. Kaufman, N. P. McKay, M. P. Erb, S. H. Arcusa, K. J. Brown, M. E. Kirby, J. P. Marsicek, R. S. Anderson, G. Jiménez-Moreno, J. R. Rodysill, M. S. Lachniet, S. C. Fritz, J. R. Bennett, M. F. Goman, S. E. Metcalfe, J. M. Galloway, G. Schoups, D. B. Wahl, J. L. Morris, F. Staines-Urías, A. Dawson, B. N. Shuman, D. G. Gavin, J. S. Munroe, B. F. Cumming, A multiproxy database of western North American Holocene paleoclimate records. *Earth Syst. Sci. Data* **13**, 1613–1632 (2021).
26. B. Menounos, G. Osborn, J. J. Clague, B. H. Luckman, Latest Pleistocene and Holocene glacier fluctuations in western Canada. *Quat. Sci. Rev.* **28**, 2049–2074 (2009).
27. O. N. Solomina, R. S. Bradley, D. A. Hodgson, S. Ivy-Ochs, V. Jomelli, A. N. Mackintosh, A. Nesje, L. A. Owen, H. Wanner, G. C. Wiles, N. E. Young, Holocene glacier fluctuations. *Quat. Sci. Rev.* **111**, 9–34 (2015).
28. H. Wanner, J. Beer, J. Bütikofer, T. J. Crowley, U. Cubasch, J. Flückiger, H. Goosse, M. Grosjean, F. Joos, J. O. Kaplan, M. Küttel, S. A. Müller, I. C. Prentice, O. Solomina, T. F. Stocker, P. Tarasov, M. Wagner, M. Widmann, Mid- to Late Holocene climate change: An overview. *Quat. Sci. Rev.* **27**, 1791–1828 (2008).
29. A. B. Gibbons, J. D. Megeath, K. L. Pierce, Probability of moraine survival in a succession of glacial advances. *Geology* **12**, 327–330 (1984).
30. G. Osborn, B. Menounos, J. Koch, J. J. Clague, V. Vallis, Multi-proxy record of Holocene glacial history of the Spearhead and Fitzsimmons ranges, southern Coast Mountains, British Columbia. *Quat. Sci. Rev.* **26**, 479–493 (2007).
31. E. M. Leonard, The relationship between glacial activity and sediment production: Evidence from a 4450-year varve record of neoglacial sedimentation in Hector Lake, Alberta, Canada. *J. Paleolimnol.* **17**, 319–330 (1997).
32. B. Menounos, J. J. Clague, Reconstructing hydro-climatic events and glacier fluctuations over the past millennium from annually laminated sediments of Cheakamus Lake, southern Coast Mountains, British Columbia, Canada. *Quat. Sci. Rev.* **27**, 701–713 (2008).
33. J. S. Stroup, M. A. Kelly, T. V. Lowell, C. A. Smith, S. A. Beal, J. D. Landis, P. M. Tapia, Late Holocene fluctuations of Quelccaya Ice Cap, Peru, registered by nearby lake sediments. *J. Quat. Sci.* **30**, 830–840 (2015).
34. B. M. Goehring, J. M. Schaefer, C. Schluechter, N. A. Lifton, R. C. Finkel, A. J. T. Jull, N. Akcar, R. B. Alley, The Rhone Glacier was smaller than today for most of the Holocene. *Geology* **39**, 679–682 (2011).
35. A. L. Gorin, J. D. Shakun, A. G. Jones, T. M. Kennedy, S. A. Marcott, B. M. Goehring, L. K. Zoet, V. Jomelli, G. R. M. Bromley, E. I. Mateo, B. G. Mark, D. T. Rodbell, A. Gilbert, M. W. Caffee, Recent tropical Andean glacier retreat is unprecedented in the Holocene. *Science* **385**, 517–521 (2024).
36. A. G. Jones, S. A. Marcott, A. L. Gorin, T. M. Kennedy, J. D. Shakun, B. M. Goehring, B. Menounos, D. H. Clark, M. Romero, M. W. Caffee, Four North American glaciers advanced past their modern positions thousands of years apart in the Holocene. *The Cryosphere* **17**, 5459–5475 (2023).
37. I. Schimmelpfennig, J. M. Schaefer, J. Lamp, V. Godard, R. Schwartz, E. Bard, T. Tuna, N. Akçar, C. Schlüchter, S. Zimmerman, ASTER Team, Glacier response to Holocene warmth inferred from in situ ^{10}Be and ^{14}C bedrock analyses in Steingletscher's forefield (central Swiss Alps). *Clim. Past* **18**, 23–44 (2022).
38. A. C. Vickers, J. D. Shakun, B. M. Goehring, A. Gorin, M. A. Kelly, M. S. Jackson, A. Doughty, J. Russell, Similar Holocene glaciation histories in tropical South America and Africa. *Geology* **49**, 140–144 (2020).
39. National Park Service, Yosemite National Park's largest glacier stagnant (2013); www.nps.gov/yose/learn/news/lyellglacier.htm.
40. H. J. Basagic, A. G. Fountain, Quantifying 20th century glacier change in the Sierra Nevada, California. *Arct. Antarct. Alp. Res.* **43**, 317–330 (2011).
41. A. E. Putnam, G. H. Denton, J. M. Schaefer, D. J. A. Barrell, B. G. Andersen, R. C. Finkel, R. Schwartz, A. M. Doughty, M. R. Kaplan, C. Schlüchter, Glacier advance in southern middle-latitudes during the Antarctic Cold Reversal. *Nat. Geosci.* **3**, 700–704 (2010).
42. J. R. Moore, J. W. Sanders, W. E. Dietrich, S. D. Glaser, Influence of rock mass strength on the erosion rate of alpine cliffs. *Earth Surf. Process. Landf.* **34**, 1339–1352 (2009).
43. S. Ye, J. K. Cuzzone, S. A. Marcott, J. M. Licciardi, D. J. Ward, J. Heyman, D. P. Quinn, A quantitative assessment of snow shielding effects on surface exposure dating from a western North American ^{10}Be data compilation. *Quat. Geochronol.* **76**, 101440 (2023).
44. B. L. Graham, J. P. Briner, N. E. Young, A. Balter-Kennedy, M. Koppes, J. M. Schaefer, K. Poinar, E. K. Thomas, In situ ^{10}Be modeling and terrain analysis constrain subglacial quarrying and abrasion rates at Sermeq Kujalleq (Jakobshavn Isbræ), Greenland. *The Cryosphere* **17**, 4535–4547 (2023).
45. M. Dühnforth, R. S. Anderson, D. Ward, G. M. Stock, Bedrock fracture control of glacial erosion processes and rates. *Geology* **38**, 423–426 (2010).
46. J. B. Woodard, L. K. Zoet, N. R. Iverson, C. Helanow, Linking bedrock discontinuities to glacial quarrying. *Ann. Glaciol.* **60**, 66–72 (2019).
47. S. J. Cook, D. A. Swift, M. P. Kirkbride, P. G. Knight, R. I. Waller, The empirical basis for modelling glacial erosion rates. *Nat. Commun.* **11**, 759 (2020).
48. D. D. Hansen, J. P. Brooks, L. K. Zoet, N. T. Stevens, L. Smith, C. E. Bate, B. J. Jahnke, A power-based abrasion law for use in landscape evolution models. *Geology* **51**, 273–277 (2023).

49. G. Osborn, B. Menounos, C. Ryane, J. Riedel, J. J. Clague, J. Koch, D. Clark, K. Scott, P. T. Davis, Latest Pleistocene and Holocene glacier fluctuations on Mount Baker, Washington. *Quat. Sci. Rev.* **49**, 33–51 (2012).
50. J. J. Clague, B. Menounos, G. Osborn, B. H. Luckman, J. Koch, Nomenclature and resolution in Holocene glacial chronologies. *Quat. Sci. Rev.* **28**, 2231–2238 (2009).
51. C. C. Routson, N. P. McKay, D. S. Kaufman, M. P. Erb, H. Goosse, B. N. Shuman, J. R. Rodysill, T. Ault, Mid-latitude net precipitation decreased with Arctic warming during the Holocene. *Nature* **568**, 83–87 (2019).
52. D. Kaufman, N. McKay, C. Routson, M. Erb, C. Dätwyler, P. S. Sommer, O. Heiri, B. Davis, Holocene global mean surface temperature, a multi-method reconstruction approach. *Sci. Data* **7**, 201 (2020).
53. S. A. Marcott, J. D. Shakun, P. U. Clark, A. C. Mix, A reconstruction of regional and global temperature for the past 11,300 years. *Science* **339**, 1198–1201 (2013).
54. A. M. Barth, E. G. Ceperley, C. Vavrus, S. A. Marcott, J. D. Shakun, M. W. Caffee, ^{10}Be age control of glaciation in the Beartooth Mountains, USA, from the latest Pleistocene through the Holocene. *Geochronology* **4**, 731–743 (2022).
55. L. S. Anderson, R. S. Anderson, Modeling debris-covered glaciers: Response to steady debris deposition. *The Cryosphere* **10**, 1105–1124 (2016).
56. I. Delaney, L. S. Anderson, Debris cover limits subglacial erosion and promotes till accumulation. *Geophys. Res. Lett.* **49**, e2022GL099049 (2022).
57. J. S. Pigati, K. B. Springer, J. S. Honke, D. Wahl, M. R. Champagne, S. R. H. Zimmerman, H. J. Gray, V. L. Santucci, D. Odess, D. Bustos, M. R. Bennett, Independent age estimates resolve the controversy of ancient human footprints at White Sands. *Science* **382**, 73–75 (2023).
58. N. J. Chellman, G. T. Pederson, C. M. Lee, D. B. McWethy, K. Puseman, J. R. Stone, S. R. Brown, J. R. McConnell, High elevation ice patch documents Holocene climate variability in the northern Rocky Mountains. *Quat. Sci. Rev.* **3**, 100021 (2021).
59. E. G. Ceperley, S. A. Marcott, J. E. Rawling, L. K. Zoet, S. R. H. Zimmerman, The role of permafrost on the morphology of an MIS 3 moraine from the southern Laurentide Ice Sheet. *Geology* **47**, 440–444 (2019).
60. L. B. Corbett, P. R. Bierman, D. H. Rood, An approach for optimizing in situ cosmogenic ^{10}Be sample preparation. *Quat. Geochronol.* **33**, 24–34 (2016).
61. R. G. Ditchburn, N. E. Whitehead, *Proceedings of the 3rd workshop of the South Pacific Environmental Radioactivity Association (SPERA)*, Australia, 1994.
62. N. Lifton, J. Wilson, A. Koester, Technical note: Studying lithium metaborate fluxes and extraction protocols with a new, fully automated in situ cosmogenic ^{14}C processing system at PRIME Lab. *Geochronology* **5**, 361–375 (2023).
63. G. Balco, J. O. Stone, N. A. Lifton, T. J. Dunai, A complete and easily accessible means of calculating surface exposure ages or erosion rates from ^{10}Be and ^{26}Al measurements. *Quat. Geochronol.* **3**, 174–195 (2008).
64. N. Lifton, T. Sato, T. J. Dunai, Scaling in situ cosmogenic nuclide production rates using analytical approximations to atmospheric cosmic-ray fluxes. *Earth Planet. Sci. Lett.* **386**, 149–160 (2014).
65. B. Borchers, S. Marrero, G. Balco, M. Caffee, B. Goehring, N. Lifton, K. Nishiizumi, F. Phillips, J. Schaefer, J. Stone, Geological calibration of spallation production rates in the CRONUS-Earth project. *Quat. Geochronol.* **31**, 188–198 (2016).
66. R. G. I. RGI Consortium, Randolph Glacier Inventory 6.0, NSIDC (2017); https://doi.org/10.7265/N5-RGI-60.
67. J. Laskar, P. Robutel, F. Joutel, M. Gastineau, A. C. M. Correia, B. Levrard, A long-term numerical solution for the insolation quantities of the Earth. *A&A* **428**, 261–285 (2004).
68. G. Balco, N. Brown, K. Nichols, R. A. Venturelli, J. Adams, S. Braddock, S. Campbell, B. Goehring, J. S. Johnson, D. H. Rood, K. Wilcken, B. Hall, J. Woodward, Reversible ice sheet thinning in the Amundsen Sea Embayment during the Late Holocene. *The Cryosphere* **17**, 1787–1801 (2023).
69. M. Blaauw, J. A. Christen, Flexible paleoclimate age-depth models using an autoregressive gamma process. *Bayesian Anal.* **6**, 457–474 (2011).

Acknowledgments: We thank the United States Forest Service and the National Park Service; J. DeMarines, C. Moeckel, and A. Tholt for field assistance; S. Bushmaker for sample processing; P. Moreno-Yaeger for assistance in mineral separation; G. Balco and the ICE-D cosmogenic-nuclide exposure-age database; D. Clark, D. Larsen, C. Moy, I. Doyle, and S. Crump for conversations; and the reviewers for improving the manuscript. This work was prepared, in part, by LLNL (LLNL-JRNL-2006519) under contract DE-AC52-07NA27344. **Funding:** This work was funded by the National Science Foundation grants EAR-1805620 (S.A.M., B.M.G., and J.D.S.) and EAR-2303293 (S.A.M. and N.A.L.), the Geological Society of America graduate student research grant (A.G.J.), the University of Wisconsin-Madison Department of Geoscience research grant (A.G.J.), and the Lawrence Livermore National Laboratory LDRD grant 14-LW-091 (S.R.H.Z.). **Author contributions:** Conceptualization: A.G.J., S.A.M., B.M.G., A.L.G., and G.M.S. Methodology: S.A.M., N.A.L., M.A.C., A.L.G., B.M.G., and A.G.J. Software: A.L.G., N.A.L., and M.A.C. Validation: A.G.J., S.A.M., M.A.C., and A.J.H. Formal analysis: A.G.J., N.A.L., and A.L.G. Investigation: A.G.J., N.A.L., G.M.S., A.L.G., A.J.H., S.R.H.Z., B.M.G., and T.M.K. Resources: S.A.M., A.J.H., M.A.C., N.A.L., and T.M.K. Data curation: A.G.J., S.A.M., N.A.L., and M.A.C. Writing—original draft: A.G.J. and S.A.M. Writing—review and editing: A.G.J., S.A.M., J.D.S., M.A.C., A.L.G., A.J.H., N.A.L., G.M.S., S.R.H.Z., and B.M.G. Visualization: A.G.J. and N.A.L. Supervision: S.A.M. and N.A.L. Project administration: A.G.J. and S.A.M. Funding acquisition: S.A.M., N.A.L., S.R.H.Z., and M.A.C. **Competing interests:** The authors declare that they have no competing interests. **Data and materials availability:** All cosmogenic nuclide data are available in the main text and the Supplementary Materials. These data are also available on the ICE-D cosmogenic-nuclide exposure-age database (https://version2.ice-d.org/). Monte Carlo forward model code is available at https://doi.org/10.1130/GEOL.S.12915737 (*38*).

Submitted 2 June 2025
Accepted 29 August 2025
Published 1 October 2025
10.1126/sciadv.adx9442